Impact of cancer-associated fibroblasts on tumour micro-environment heterogeneity in response to chemotherapy

Tim van der Plas

Translational Research in Tumour Microenvironment laboratory

Daily supervisor: Jordi Badia-Ramentol, PhD

Project supervisor: Alexandre Calon, PhD

Examiner: Onno Kranenburg, PhD, prof.

29/03/2023

Abstract

Despite many advances in surgery, chemotherapy and personalised medicine, colorectal cancer (CRC) remains the third leading cause of cancer-related deaths worldwide. After curative treatment, 30% to 40% of patients relapse. The tumour micro-environment (TME), and the cancer-associated fibroblasts (CAFs) that reside in it, play a major role in CRC tumour progression and resistance to treatment.

Here, we analyse two CAF subtypes with a mutually exclusive gene expression pattern that were identified from a biobank of patient-derived CAFs. CAFs from these subtypes are co-cultured in a 3D TME model with patient-derived organoids (PDOs) from CRC tumours to assess their influence on tumour growth via a luciferase reporter. Furthermore, tumour growth and gene expression dynamics are monitored upon treatment of the model with chemotherapy. We find that certain CAFs from both subtypes increase tumour growth and drive resistance to therapy. In addition, we see how CAFs from one subtype drive aggregation of the PDOs in our TME model. Lastly, we show how healthy fibroblasts in co-culture with PDOs increase expression of CAF markers upon oxaliplatin treatment.

Taken together, this study underlines the bidirectional interactions of tumour cells and CAFs in the TME of CRC carcinomas to drive disease progression and resistance to treatment. These findings merit further research to distinguish CAF clusters that drive these interactions and discover new biomarkers.

Table of Contents

Lay summary

Despite advances in surgery and chemotherapy, colorectal cancer (CRC) remains the third leading cause of cancer-related deaths worldwide, and yearly diagnoses are predicted to rise to rise to 3,16 million by 2040. Survival is lowest when the tumour advances to an aggressive stage and tumour cells invade other organs. On the other hand, when the tumour is discovered while still localised in the colorectal tissue, it can be treated with surgery and chemotherapy. While survival numbers are greater in this condition, still 30 to 40% of patients redevelop tumours after this treatment. Over the past decades, increasing evidence points to an important role of healthy body cells that are localised around the tumour in development of resistance to treatment. This environment of cells around the tumour, named the tumour micro-environment (TME), consists for a large part of fibroblast cells. These cancer-associated fibroblasts (CAFs) interact with the tumour cells and can drive progression of the disease.

In this study, we analyse many different CAFs that were derived from patient tumours after surgery. By measuring gene expression of these different CAFs, we discover specific gene expression profiles that distinguish 6 subpopulations of CAFs. Cluster 1 and 3 show the most differences and have distinct gene expression patterns. On top of that, cluster 3 CAFs were derived from more aggressive tumours, while cluster 1 CAFs were derived from less advanced tumours.

To investigate the effect that these different clusters have on tumour cells, we use a model of the TME by culturing these CAFs together with patient-derived tumour cells in a 3D environment. By doing this, we analyse whether tumour cells grown with certain CAFs around them grow faster and are more resistant to chemotherapy. We show that certain combinations of CAFs and tumour cells grow faster than others, yet we do not see a specific growth dynamic related to the CAF clusters.

Interestingly, we notice how CAFs from cluster 3 affect the distribution of tumour cells in our model, driving the tumour cells to aggregate together in the centre of the model, while cultures of tumour cells with cluster 1 CAFs do not show this dynamic. This points to a possible influence of the cluster 3 CAFs on the composition of the model and further underlines the central role of CAFs in the TME.

Lastly, we observe how healthy fibroblasts change their gene expression towards a state that is similar to CAFs, when they are cultured together with tumour cells. This illustrates the crosstalk between the tumour cells and fibroblasts in the TME, and the role that tumour cells have in activating fibroblasts.

Taken together, this study shows how interactions between CAFs and tumour cells affect the growth of colorectal cancer tumour cells, as well as their expression patterns. Further research to distinguish CAF clusters that play important roles in the TME to protect the tumour against treatment are an important next step to discover new targets for treatment and improving localised CRC care.

Introduction

Despite many advances in surgery, chemotherapy and personalised medicine, colorectal cancer (CRC) remains the third leading cause of cancer-related deaths worldwide.[1] In 2020, CRC accounted for 1,93 million cancer diagnoses (10% of global cancer diagnoses) and 0,94 million cancer deaths (9,4% of global cancer deaths) among all genders, ranking third globally.[1] In fact, global CRC prevalence has been increasing alarmingly in the recent years, with the number of diagnoses yearly predicted to rise to 3,16 million in 2040.[2]

Mechanism and diagnosis

CRC develops from the accumulation of mutations in key oncogenes occurring in epithelial cells of the colon and rectal lining. Most often, the first or "gatekeeping" alterations occur in the APC gene, which gives a selective growth advantage over the healthy epithelial cells, thus creating an adenoma.[3] Subsequent mutations in tumour driver genes such as KRAS, PIK3CA, SMAD4 or TP53 will create a malignant tumour with potential to metastasize.[4]

Upon diagnosis, tumour progression is defined by TNM classification as developed by the American Joint Committee on Cancer (AJCC), based on tumour size (T), lymph node (N) and distant organ invasion (M).[5] Early carcinomas can be classified as stage 0, I or II, depending on size and which tissue layers the tumour has invaded, whereas spreading to lymph nodes or distant organs respectively classifies as stage III and IV.[5] This AJCC staging system is one of the major determinants of prognosis.[6]

CRC patients often start showing symptoms when the disease reaches an advanced stage, becoming more aggressive and malignant. Symptoms may include unexpected weight loss, changes in bowel habits, abdominal pain, anaemia, and rectal bleeding.[7] [8] Additional risk factors such as lifestyle, chronic inflammatory bowel disease or genetic predisposition are also taken into account to identify those patients that require further investigation via colonoscopy.[2] In order to diagnose patients before progression of the disease, population-based CRC screening programs are in effect in many countries. These programs mostly aim to test stool samples of people between 50-75 years of age for small amounts of blood.[7] Colonoscopy, biopsy analysis and complementary computerised tomography (CT) can subsequently confirm colorectal cancer diagnosis and identify cancer stage and molecular subtype to inform treatment strategies.[9]

At the molecular level, CRC can be categorised in four consensus molecular subtypes (CMSs), depending on the molecular features of the tumour.[10] [11] The aforementioned accumulation of mutations results in canonical carcinomas (CMS2), while a further combination of copy number variation events and KRAS mutations resulting in metabolic deregulation are typical of CMS3 carcinomas. CMS4 tumours are characterised by a high infiltration of stromal cells, and gene expression signatures correspond to activation of the transforming growth factor-β (TGFβ) pathway and extracellular matrix remodelling. Alternatively, CRC tumours with microsatellite instability (MSI), which have a distinctive pattern associated with hypermutation and hypermethylation, are classified as CMS1. Of these subtypes, patients with CMS4 tumours exhibit the worst relapse-free and overall survival and tend to be diagnosed at advanced stages III and IV.[10]

Treatment

Advancements over the past decades have increased the understanding of the pathophysiology of CRC and improved the number and quality of treatment options, doubling the overall survival of advanced CRC to three years.[8] Upon early detection at stage 0, polyps can be removed endoscopically. For stage I, II and III CRC tumours, the main treatment strategy is resection surgery. Here, the prognosis of disease is strongly related to surgery quality as assessed by analysing the resected tumour.[12] [13] In addition to surgery, stage III

tumours are treated with adjuvant chemotherapy. For over 50 years, 5-Fluorouracil (5FU, pyrimidine antagonist that interferes with DNA synthesis) has been the conventional first-line chemotherapy choice.[9] 5FU is generally combined with leucovorin (enhances cytotoxic inhibitory effect of 5FU). In addition, fluorouracil-leucovorin can be combined with oxaliplatin (FOLFOX), irinotecan (FOLFIRI), or both (FOLFOXIRI).[14] Successful tumour resection combined with adjuvant chemotherapy for stage III CRC decreases risk of recurrence and subsequent metastases from 25-50% to 20-30%.[9]

For metastatic stage IV CRC, disease management mainly focuses on chemotherapy, and can additionally involve ablation of metastasis sites.[15] Metastasis ablation treatments, such as metastasis resection surgery or radiotherapy, are preferential in liver metastasis, whereas lung and peritoneal metastases are more difficult to treat locally.[8 9] Cancer progression is monitored every 2 to 3 months with CT scans. Therapy is continued upon tumour regression or stable disease, as long as it has been well tolerated. Alternatively, patients with disease progression switch to next-line treatment regimens.[8]

In this case, chemotherapy treatments are combined with biological agents in targeted therapy. Targeted therapy efficiency relies on the molecular characteristics of the tumour. For instance, 80% of CRCs express or overexpress EGFR, which correlates with a reduced survival and an increased risk of metastasis.[16] EGFR antibodies such as Cetuximab and Panitumumab increase progression-free and overall survival.[17] On the other hand, in roughly half of all CRC cases RAS is mutated, whereby the RAS GTPase is constitutively active. Activated RAS induces many tumorigenic intracellular signalling pathways and renders antiEGFR therapies ineffective. Another protein viable for targeted therapy, is key tumour angiogenesis effector VEFG-A. While the precise mechanisms are yet to be fully defined, specific VEGF-A therapies such as Bevacizumab and Aflibercept have shown to be effective.[18 19]

CRC treatment remains difficult given the heterogeneous nature of the tumour. This stresses the importance of classifying tumours on a genetic and molecular basis, such as the CMS system proposes. For example, CMS2 (canonical) tumours, which are most prevalent (37% of total) tumours, exhibit superior long-term survival compared to the other subtypes.[10] Contrarily, CMS4 (mesenchymal) tumours (23% of total) account for the worst relapse free and overall survival numbers. Such a contrast results from differences in genetic characteristics, but also due to extensive variability in the make-up of the tumour micro-environment (TME).[20] CMS4 tumours are characterised by high stromal infiltration and intermediate immune infiltration from the TME.[21] This infiltration can promote important cancer progression processes, such as TGFβ activation and angiogenesis, underlining the important role of the TME in tumour development.[20]

Tumour microenvironment

CRC tumours are under constant influence of the wide array of non-malignant cells that constitute the TME. Most notable cell populations in the TME include immune cells, endothelial cells, and cancer-associated fibroblasts (CAFs). Fibroblasts in the stromal compartment of the colon mucosa crosstalk with the epithelial compartment to impose tissue integrity. In cancerous tissue this crosstalk is altered, resulting in an “efferent” and “afferent” pathway of tumorigenesis.[22] The efferent pathway describes the role of cancerous epithelial cells in driving fibroblast differentiation into CAFs, by secretion of a host of effectors, including platelet-derived growth factor (PDGF), fibroblast growth factor 2 (FGF2) and TGFβ.[23 24] The afferent pathway describes how, when differentiated, CAFs can produce and secrete many factors with either tumour-restraining or tumour-promoting effects.[22 25 26] While genetically much more stable compared to the epithelial tumour cells, CAFs are very heterogeneous and can therefore elicit a wide spectrum of functions.[27 28 29] TGFβ is a main

effector for this influence, as it drives tumour-initiating capacity of CAFs for the tumour cells, while inhibition of its signalling has been shown to prevent progression to metastasis in immunodeficient mice.[30] In contrast, TGFβ affects tumour cells directly by slowing down proliferation, leading to selective pressure of mutations in sensitivity to TGFβ in tumours.[31] Interestingly, TGFβ expression is elevated in all CRC subtypes related to poor prognosis.[31] On top of that, several other genes used to classify tumours and predict poor prognosis are specifically expressed by stromal cells, particularly by CAFs, suggesting that CAF gene expression might influence the whole tumour expression profiles.[31]
More recently, our lab has shown that chemotherapy treatment has an influence on gene expression changes in the TME as well.[32] Remarkably, oxaliplatin was shown to accumulate in the stromal compartment of the TME, remaining detectable until long after treatment ended. Oxaliplatin accumulation increased TGFβ expression, upregulating IL11 and POSTN, genes associated with tumour initiation and therapy resistance.[23]
Taken together, CAFs in the TME have an important influence on therapy resistance of the tumour. Further investigation into identifying distinct subtypes of CAFs in CRC patients would allow for better understanding of their role in the TME, in turn possibly identifying subtypes that provide novel biomarkers of resistance to therapy.

In this report, we analyse CAFs derived from CRC patients to uncover their characteristics and their influence on tumour cell dynamics in a 3D co-culture TME model previously described by our lab.[33] We analyse CAF expression patterns previously generated in our lab to investigate the presence of CAF subtypes in the patient-derived CAF lines. In a 3D setting, patient-derived organoids (PDOs) of CRC patients are cultured together with CAFs to examine the influence of the CAFs on tumour growth via a luciferase reporter, and on gene expression dynamics via quantitative real-time PCR. In addition, co-cultures are treated with chemotherapy agent oxaliplatin to study tumour growth and expression dynamics of CAFs and PDOs and assess resistance to treatment. This research will continue efforts to identify distinct CAF clusters present in CRC patient samples and will additionally investigate the effect of CAFs on tumour cell growth and expression dynamics, as well as treatment resistance. Research on CAF clusters and their influence is essential in expanding knowledge on the role of the tumour microenvironment in the heterogeneity of tumours and resistance to therapy. On top of that, by uncovering certain CAF clusters associated with poor prognosis and their biomarkers could have predictive power for targeted therapy.

Results

For a comprehensive investigation into the role of CAFs in CRC tumours, our lab constituted a biobank of patient-derived organoids (PDOs) and patient-derived CAFs over the past years. In order to study tumour cell growth, we infected three stably growing PDOs with a construct encoding a fusion protein of mCherry coupled to a firefly Luciferase. **(Figure 1A)** The luciferase enzyme allows for analysis of bioluminescence upon addition of luciferin to the culture medium, effectively reporting tumour growth.
Once homogeneous mCherry-Luciferase expression was established, we first assessed the cytostatic effects of TGFβ on PDOs by culturing them in the presence of either TGFβ or A83, a TGFβ receptor I inhibitor. PDxO06 exhibited increased growth when TGFβ signalling was inhibited. **(Figure 1B, supplementary figure 1)** To a lesser extent, similar dynamics were observed in PDO13 and PDO03 when adding A83. Addition of TGFβ significantly reduced tumour growth for all three PDOs.

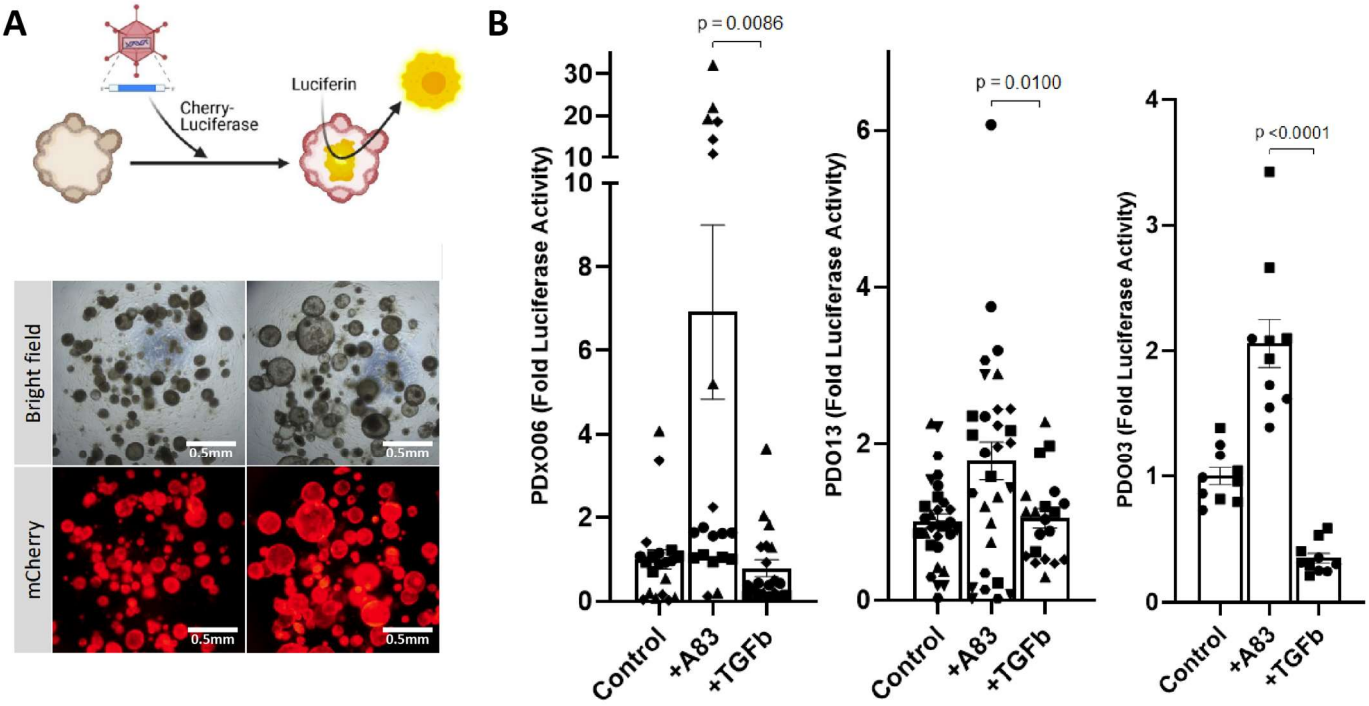

Figure 1: Characterization of PDOs from the biobank derived from CRC tumour biopsies.
A) Schematic representation of lentiviral infection of PDOs with the mCherry-Luciferase construct, with representative bright field images of PDOs and their mCherry expression illustrated below. ***Note: this panel was compiled by daily supervisor J.B.R.*** **B)** Tumour growth of PDxO06, PDO13 and PDO03, as reported by fold increase in relative light units. PDO cultures were exposed to either a control medium, or medium containing A83 or TGFβ. Columns are mean ± SEM. Each point represents individual co-cultures. Point shape corresponds to technical replicates.

To investigate patterns of gene expression in the TME, the 57 CAFs from our biobank were previously analysed for a wide array of genes implicated in CAF subtyping.[36 37] Clustering the CAFs based on their expression dynamics for this gene set resulted in a distinction of 6 separate CAF clusters. **(Figure 2A)** Cluster 1 and 3 are the most abundant CAF clusters in our biobank and present a mutually exclusive gene expression pattern. When we compare these clusters to the CRC stage they were derived from, we see a remarkable association to certain AJCC stages. **(Figure 2B)** Cluster 1 CAFs are mostly found in less advanced, stage I and II tumours, while cluster 3 CAFs are predominantly represented in stage III and metastasised tumours. Given their clear distinction in both gene expression signature and cancer stage association, while also being the most abundant clusters, we considered CAF clusters 1 and 3 as the first candidates for further analysis.

To assess whether these two distinct CAF clusters would also influence tumour cells differently, we went on to establish 3D co-cultures of PDOs with CAFs. We analysed tumour growth by means of luciferase activity, measured in relative light units emitted by the infected PDOs when supplied with luciferin. Tumour growth was assessed in PDOs in co-culture with either normal fibroblasts (NF2, derived from healthy mucosa), cluster 1 CAFs (CAF17 & CAF19), or cluster 3 CAFs (CAF12 & CAF38). **(Figure 3A,B).** For this setting, we used a starvation medium to allow CAFs to provide tumour cells with the required niche factors. After 21 days of co-culture, PDxO06 showed comparable growth dynamics with each of the CAFs. PDO03 did not grow with CAF19, while growth rate was increased when co-cultured with CAF12 and CAF17. **(Figure 3B.2)**
Next, we compared growth dynamics upon oxaliplatin treatment. **(Figure 3C)** From day 4 until day 7, co-cultures were treated to 2µl/ml of oxaliplatin. PDO13 was unable to grow when subjected to the

chemotherapy, while PDO03 exhibited reduced growth for all combinations. For PDxO06, most co-cultures were unable to grow after chemotherapy, however, CAF12 and CAF19 co-cultures resisted therapy and grew significantly, albeit at a reduced rate compared to the untreated culture. **(Figure 3C.1)** Next, we introduced a second round of oxaliplatin, from day 11 until day 14, with the aim to assess acquired resistance to therapy after the first treatment. **(Figure 3D)** PDxO06 and PDO03 growth is further impaired by the second treatment, and they are unable to recover.

In order to see the growth differences more clearly between the different co-cultures, we compared luciferase activity at day 14, as measurements on this day were the most accurate and reliable of all timepoints after the treatments. **(Figure 3E,F, supplementary figure 2)** PDxO06 in co-culture with CAF12 resisted to oxaliplatin. Also, PDO03 grew mostly with CAF17 and CAF12, and resisted therapy when in co-culture with CAF17. **(Figure 3F)**

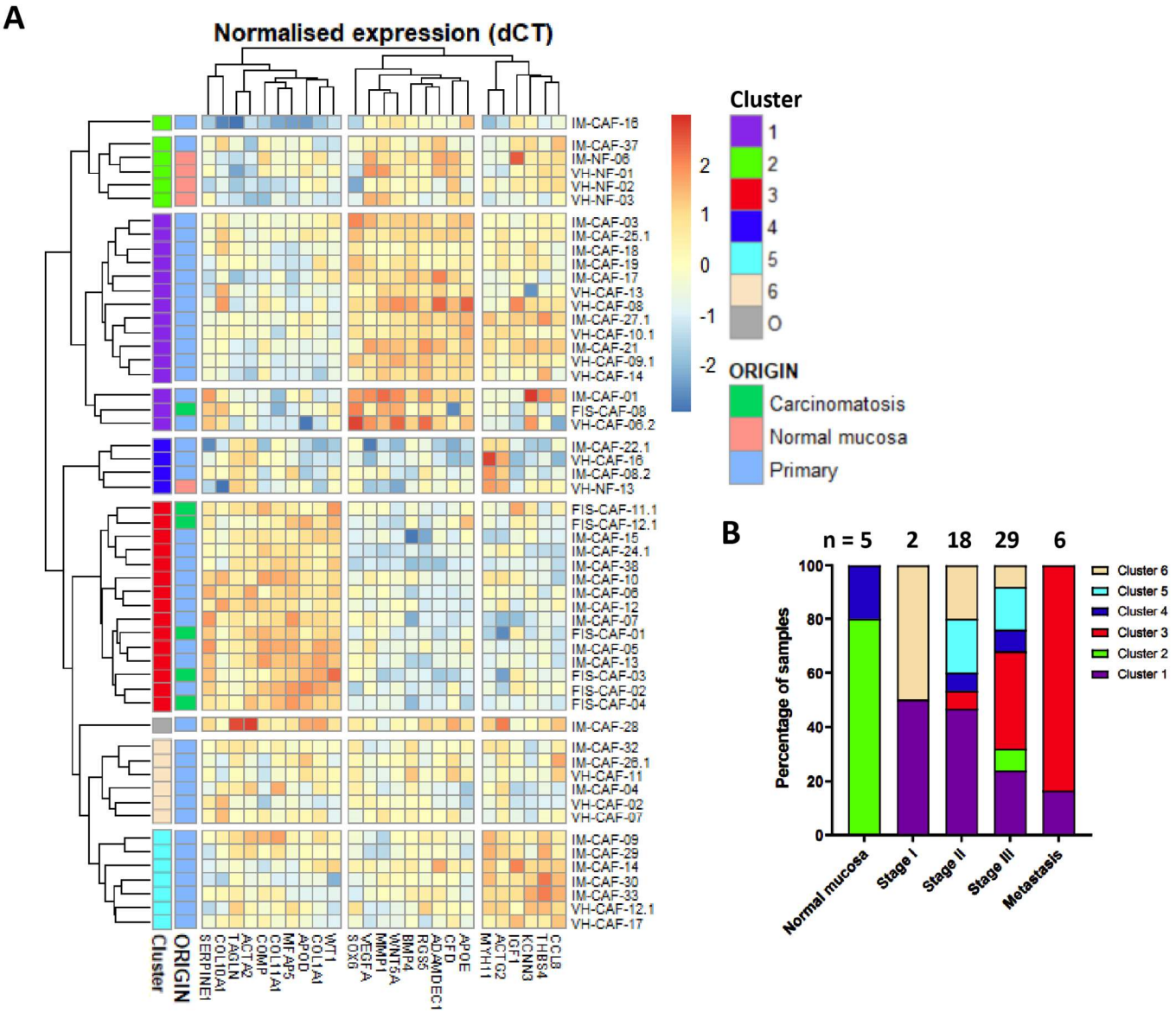

Figure 2: CAFs clustered based on gene expression.

A) Scaled heatmap of gene expression of CAFs from our biobank. Euclidian clustering was applied to identify 6 clusters of CAFs ***Note: gene expression data collection was conducted by J.B.R. and heatmap visualisation was done by T.P.*** **B)** Cluster representation in normal mucosa and different CRC stages. Number of CAFs in each stage is indicated above the columns. ***Note: this panel was compiled by J.B.R.***

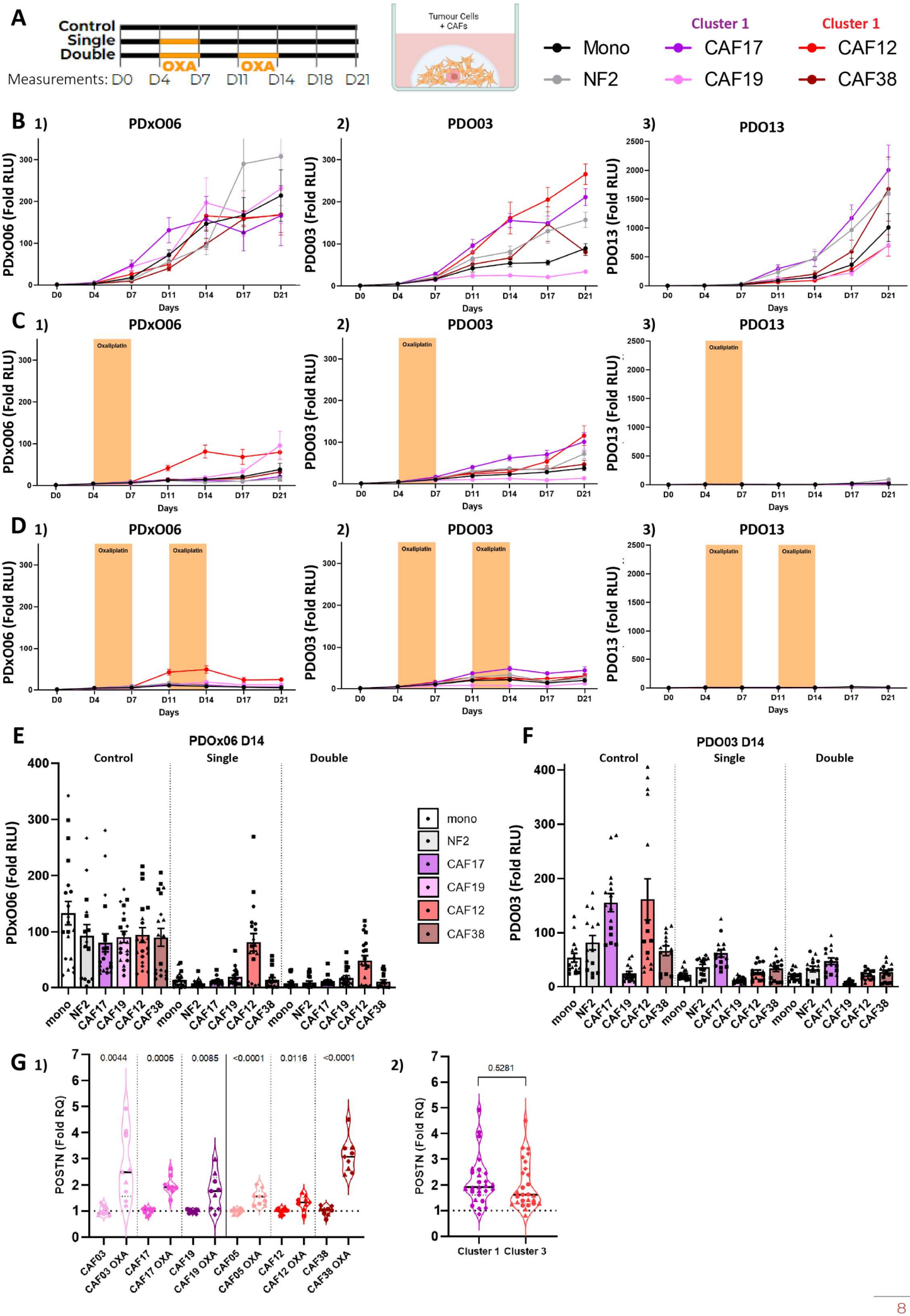
A
Control
Single
Double
OXA
OXA
Measurements: D0 D4 D7 D11 D14 D18 D21
Tumour Cells + CAFs
Mono
NF2
Cluster 1
CAF17
CAF19
Cluster 1
CAF12
CAF38
B 1) PDxO06
2) PDO03
3) PDO13
PDxO06 (Fold RLU)
PDO03 (Fold RLU)
PDO13 (Fold RLU)
Days
C 1) PDxO06
2) PDO03
3) PDO13
Oxaliplatin
D 1) PDxO06
2) PDO03
3) PDO13
Oxaliplatin
E PDOx06 D14
Control
Single
Double
PDxO06 (Fold RLU)
mono
NF2
CAF17
CAF19
CAF12
CAF38
F PDO03 D14
Control
Single
Double
PDO03 (Fold RLU)
G 1)
POSTN (Fold RQ)
0.0044
0.0005
0.0085
<0.0001
0.0116
<0.0001
CAF03
CAF03 OXA
CAF17
CAF17 OXA
CAF19
CAF19 OXA
CAF05
CAF05 OXA
CAF12
CAF12 OXA
CAF38
CAF38 OXA
2)
0.5281
Cluster 1
Cluster 3

Figure 3: Growth dynamics of tumour cells in co-culture with CAFs from clusters 1 and 3.
A) Left: Schematic representation of experiment setup and treatments. Right: Legend for the CAFs depicted in B), C) and D). **B-D)** Tumour growth plots of PDxO06 (1), PDO03 (2) and PDO13 (3), as reported by fold increase in relative light units in untreated conditions (B) or treated with a single dose (C) or two doses of oxaliplatin (D). Colours correspond to the legend in A). Each point shows a mean value of three replicates ± SEM. **E, F)** Tumour growth after 14 days for PDxO06 (E) and PDO03 (F) under control, single or double oxaliplatin treatment, as reported by fold increase in relative light units. Each point presents an individual co-culture, with point shape corresponding to each replicate. Columns show mean values ± SEM. **G)** Violin plots (median ± quartiles) of fold change relative expression of POSTN in CAFs from clusters 1 and 3, while untreated or treated with oxaliplatin (OXA). Colours correspond to their respective cluster (1=purple, 3=red), point shape corresponds to each replicate experiment, while points from the same replicate represent three internal qPCR replicates. In 2), CAFs from the same cluster are combined for cluster comparison. P values resulting from unpaired t-tests with Welch's correction are indicated above.

We next analysed gene expression differences for POSTN, a gene implicated in therapy resistance [32], in CAFs from both clusters (cluster 1: CAF03, CAF17, CAF19, cluster 3: CAF05, CAF12, CAF38) after oxaliplatin treatment and found that all CAFs significantly increased POSTN expression upon treatment with oxaliplatin. **(Figure 3G)** When directly comparing the clusters for POSTN expression after oxaliplatin treatment by combining the separate CAFs, cluster 1 tended to upregulate POSTN at a higher level compared to cluster 3, although this difference was not statistically significant.

While we did not observe a clear similarity within CAF clusters, the physical appearance of the co-cultures differed between clusters. **(Figure 4)** Remarkably, untreated PDO13 in co-culture with cluster 3 CAFs for 21 days grew in dense bundles, while co-culture with cluster 1 appears in a more spread-out formation. **(Figure 4A, B)** CAF12 (cluster 3) adopted an elongated shape and grew tightly in a clump, while CAF17 (cluster 1) hardly elongated and did not congregate.

The availability of paired PDOs and CAFs, that is, derived from a same patient, allowed us to model patient-like CAF-tumour cells interactions in vitro. Thus, we next followed PDO03 growth in co-culture with CAF03 (cluster 1), both derived from the patient 03, or in co-culture with CAF05 (cluster 3). **(Figure 5A, C)** In control conditions, PDO03 grew better when co-cultured with its paired CAF compared to CAF05. However, CAF03 nor CAF05 protected PDO03 against any form of oxaliplatin treatment. **(Figure 5B, C)** Bright field microscopy reveals a similar CAF growth pattern as previously shown for other cluster counterparts. (**Figure 5D, supplementary figure 3).**

Figure 4 (Below): Cluster-specific growth patterns of CAFs in 3D culture.
A) Bright field microscopy images of PDO13 in 3D monoculture (mono), or 3D coculture with different CAFs or normal fibroblasts (NF02) after 21 days. Clusters 1 (purple, CAF17 & CAF19, and 3 (red, CAF12 & CAF38) are indicated above. **B)** 400% crop of microscopy images showing 3D co-cultures of PDO13 with CAF17 (left, cluster 1), and IMI-CAF-12 (right, cluster 3), after 21 days of culturing, including a single oxaliplatin treatment from day 4 until day 7.

A

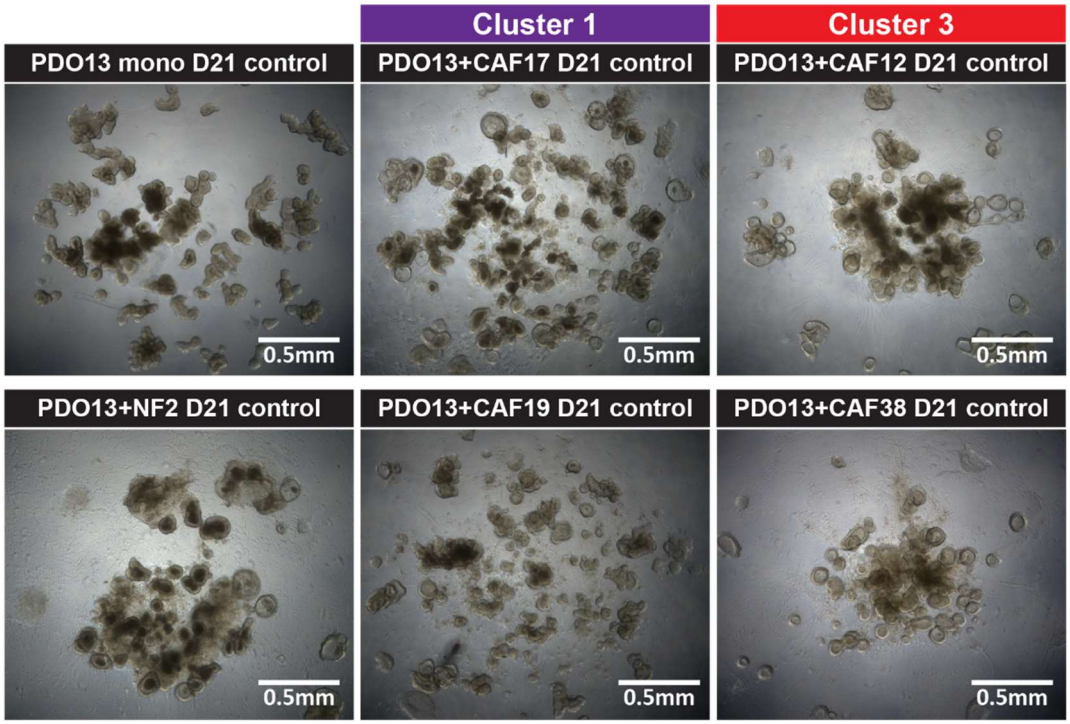

B

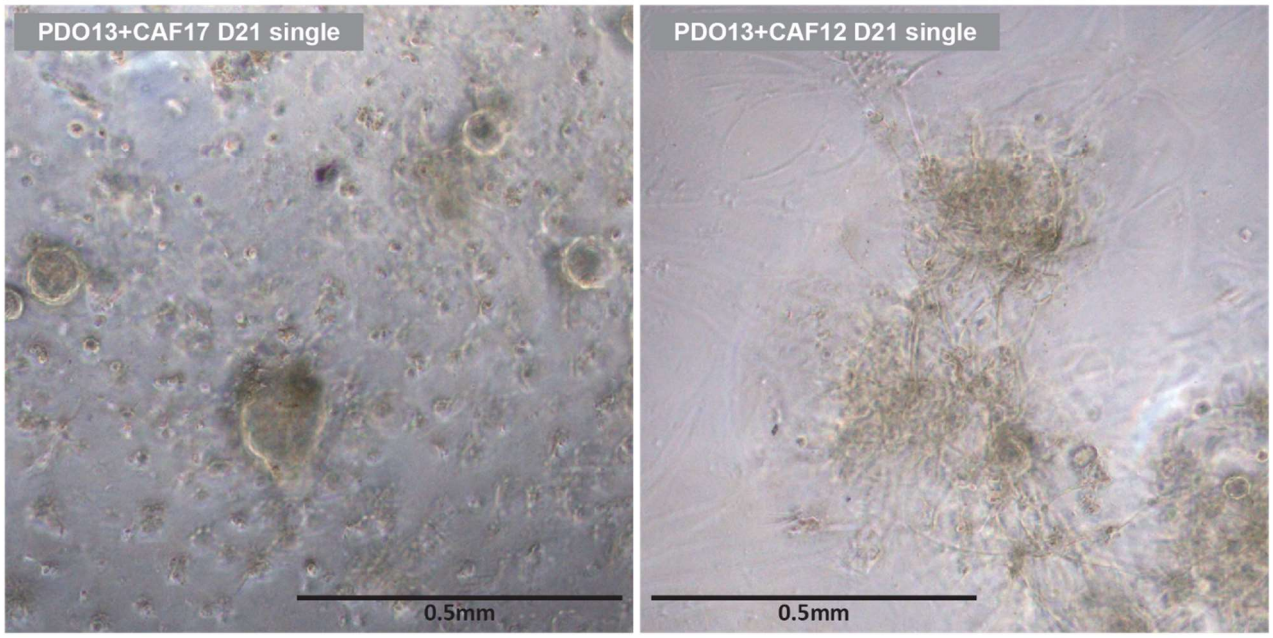

Next, we analysed gene expression dynamics of patient-like models from both cluster 1 and 3. **(Figure 6A, supplementary figure 4)** To do this, paired models from patients 03 and 05 were followed for 17 days in untreated conditions or single or double oxaliplatin treatment. For the analyses, we used EPCAM, a typical marker of epithelial cells, as a readout for tumour cell relative abundance. To determine CAFs from each cluster, we used WNT5a and MMP1 as markers of Cluster 1, and TAGLN and ACTA2 as markers for Cluster 3, as previously determined in our lab. As expected, EPCAM expression decreased upon treatment with oxaliplatin in both patient models. Cluster 1 marker expression is downregulated in the CAF05 (cluster 3) model over time, and WNT5A expression is upregulated after double oxaliplatin treatment. Interestingly, neither WNT5A and MMP1 are upregulated over time in the CAF03 (cluster 1) model, instead WNT5A is downregulated in both control and single treatment settings. TAGLN and ACTA2 are used as markers for cluster 3 CAFs and their expression increases over time in the CAF05 model with and without

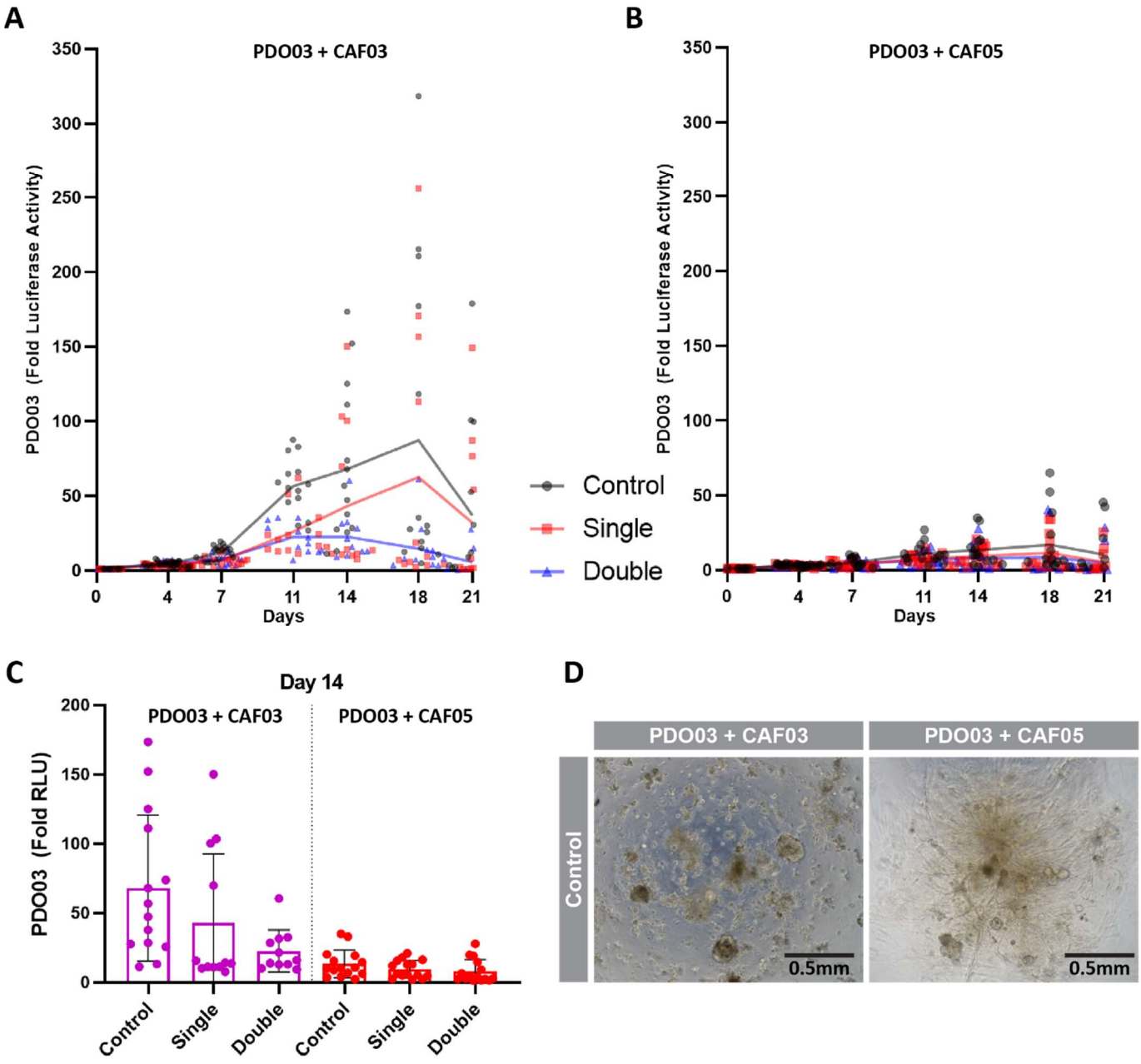

Figure 5: Growth dynamics of patient-like co-cultures of PDOs and CAFs derived from the same patient. **A-B)** Tumour growth of PDO03 when in co-culture with CAF03 (cluster 1, A), from the same patient, or CAF05 (cluster 3, B) as reported by fold increase in relative light units. Colours correspond to control, single and double oxaliplatin treatments. Each point presents an individual co-culture from a total of 3 replicates. Lines are drawn between the means of each condition to follow mean tumour growth over time. **C)** PDO03 growth at day 14 when co-cultured with CAF03 (purple) or CAF05(red), represented in violin plots (median ± quartiles) of fold luciferase activity. **D)** Bright field microscopy images of co-cultures with PDO3 and CAF03 (left) or CAF05 (right).

treatment. In the CAF03 model we do not see such increase over time in the control situation, yet both markers are upregulated over time upon oxaliplatin treatment. Additionally, POSTN and FAP expression were analysed for their implications as poor prognosis biomarkers. Interestingly, in control situations for patient model 03, expression of both genes decreased over time. After treatment with oxaliplatin, POSTN expression increased over time and FAP expression only increased in the double treatment setting. **(Supplementary figure 4C)** Conversely, for the patient 05 model, FAP expression strongly increased upon

oxaliplatin treatment. Furthermore, POSTN expression was maintained over time in the control setting, and strongly increased after double oxaliplatin treatment. **Figure 6B)**

Finally, we wanted to investigate the genetic dynamics in co-cultures of PDOs with normal healthy fibroblasts upon oxaliplatin treatments. **(Figure 6C)** When assessing gene expression of PDO13 with NF02 over time, EPCAM expression was lost after treating with oxaliplatin. Both cluster 1 markers TAGLN and ACTA2 increase expression upon treatment, and the same is observed for WNT5A, while MMP1 is increased to a lesser extent. Interestingly, both POSTN and FAP expression increased when treating with oxaliplatin. For the co-culture of PDO06 with NF02, EPCAM expression remained elevated after treatment, indicating resistance to treatment. While ACTA2 expression remained stable in control settings, TAGLN was highly increased, and both genes were upregulated after treatment. Again, WNT5A expression rose after treatment, while MMP1 expression remained stable. Similar to PDO13, in PDO06, both POSTN and FAP exhibit increased expression after treatment with oxaliplatin.

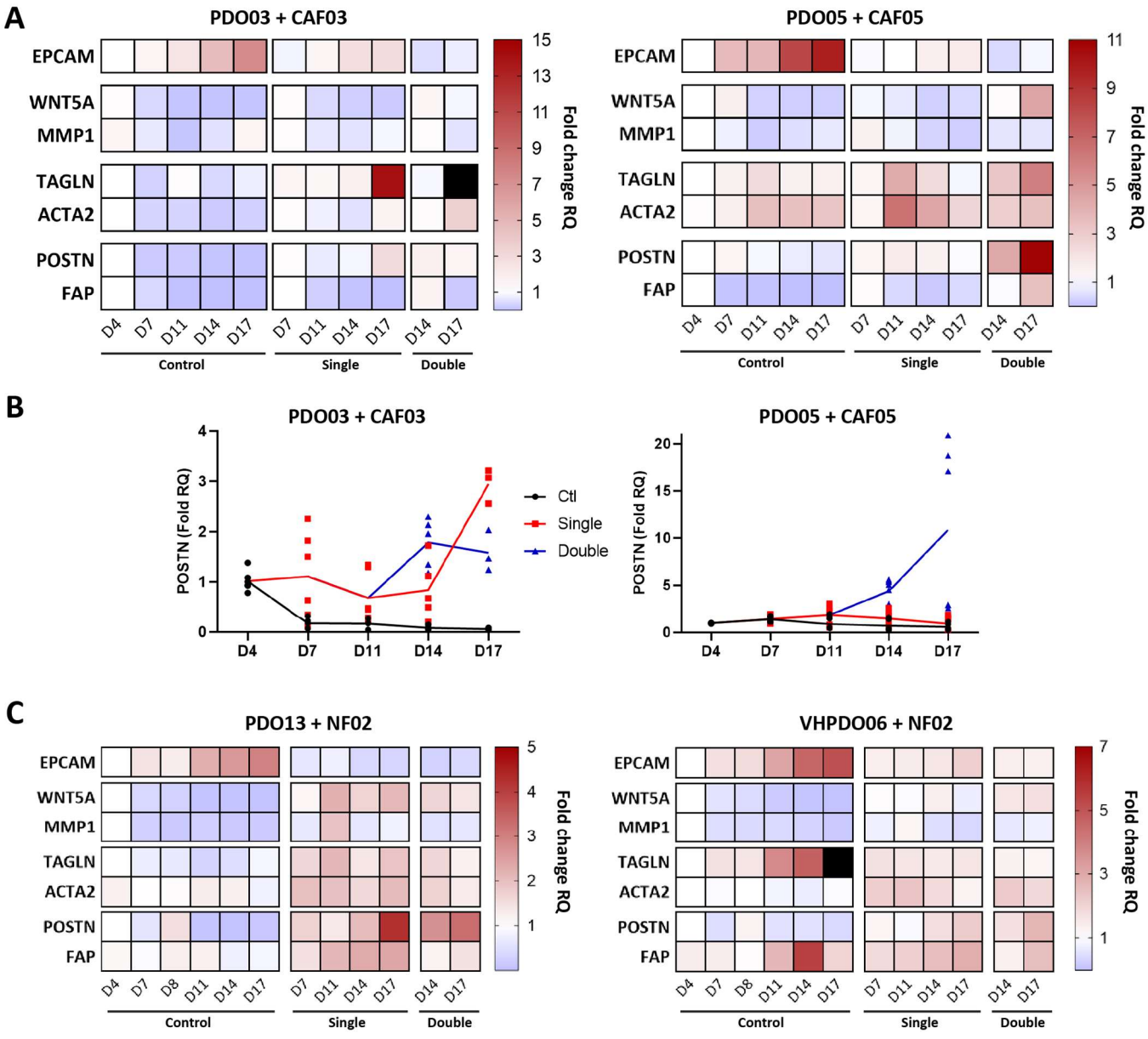

Figure 6: Gene expression dynamics of patient-like co-cultures from cluster 1 and 3.
A) Heatmap of fold change relative gene expression in patient-like co-cultures of PDO03 +CAF03 (cluster 1) and PDO05 + CAF05 (cluster 3). Timepoint and treatment conditions are indicated below. **B)** relative gene expression Fold change of POSTN along several timepoints in co-cultures of both patient-like combinations. Colours correspond to treatment condition, and points represent all qPCR replicates of 1 to 3 replicate experiments. Lines are drawn between the means of these points to monitor POSTN expression over time. **C)** Heatmap of fold change relative gene expression in co-cultures of PDO13 + NF02 and PDO06 + NF02. Timepoint and treatment conditions are indicated below.

Discussion

In this study, we reported the growth dynamics of co-cultures of PDOs with patient-derived CAFs from different CAF clusters which were identified by gene expression analysis. Specific PDO-CAF co-cultures stand out in terms of their growth dynamics over time and merit further discussion. **(Figure 3)** For instance, CAF19 was unable to support tumour growth for PDO03, while it did stimulate growth for the other PDOs. CAF12 strongly supported PDxO06 and PDO03, and was even able to protect PDxO06 against chemotherapy. CAF17 showed similar protection for PDO03, having no such effect in the other PDOs.
For the patient-like model, we see how PDO03 grows rapidly when co-cultured with CAF03 yet elicits decreased growth when this CAF is changed to CAF05. It is clear from these dynamics that there is no significant pattern of specific clusters having a certain influence. However, crosstalk between PDOs and CAFs of certain combinations can provide standout growth advantages or disadvantages for the tumour, further indicating the relevance of CAFs in the TME. Ongoing experiments including additional PDOs and more CAFs from each cluster look to provide more insight into the presence of a cluster-dependant influence on tumour growth.

In gene expression dynamics analyses of patient model co-cultures, we see expression of cluster 3 markers increasing in control conditions for a cluster 3 CAF co-culture, and cluster 3 markers upregulated in patient models from both cluster 1 and 3 upon oxaliplatin treatment. **(Figure 6)** Addtionally, common across PDOs and CAFs, is an increase in expression of POSTN and FAP when the co-cultures are treated with chemotherapy. Both genes have been implicated as predictor of poor prognosis in CRC patients.[31] [32] These results show a tendency of the expression pattern of the TME model to shift towards a signature associated with both cluster 3 TMEs and poor prognosis after chemotherapy. Additionally, we see how the expression pattern of TME models with healthy fibroblasts also shift towards a higher expression of POSTN and FAP after chemotherapy. **(Figure 6C)** On top of that, the TME upregulates expression of our CAF clusters markers. Cluster 3 markers TAGLN and ACTA2 are most notably increased and indicate a possible activation of the healthy fibroblasts to transition to become CAFs. Interestingly, we see how VHPDO06 already has this effect on healthy fibroblasts without treatment being involved, further implying the bidirectional interactions in the TME.

Additionally, we observed an interesting difference between growth dynamics of CAFs from cluster 1 and 3, as illustrated in microscopy images. **(Figure 4, 5D, supplemental figure 3)** CAFs from cluster 3 were able to elongate and congregate in the 3D gel droplet, while CAFs from cluster 1 did not elongate and remained spread through the droplet. Since fibroblasts have an essential role in modelling the extracellular matrix (ECM), a role that is affected upon tumour formation, it is possible that our CAF clusters affect the droplet

matrix differently.[25 26] This possible influence on the composition of the droplet matrix influences PDO growth in terms of their localization towards the centre of the droplet in cluster 3 co-cultures. However, we did not find clear indications of this growth behaviour effecting expression or resistance to therapy in a cluster-dependant manner consistent across all PDOs. **(Figure 2, 5, 6)** Further analysis of cluster-dependant CAF growth dynamics over time in 3D matrix models is required to draw conclusions on the precise differences between clusters and their influence on PDOs.

Relatedly, it can be questioned whether all CAFs remain viable, proliferative, and representative when cultured in 3D matrix models. The observed differential growth dynamics discussed above could be explained if certain CAFs are simply unable to remain active in the 3D setting. This can be followed up by comparing fibroblastic, proliferation and senescence marker expressions in CAFs in a 2D and 3D setting. Furthermore, we are currently infecting the CAFs in our biobank with a GFP-hTERT (Telomerase Reverse Transcriptase) construct. CAFs stably expressing this construct will both be immortalised by preventing telomere-controlled senescence, and their growth dynamics in both 2D and 3D setting can be monitored via the GFP fluorophore to identify possible differences in droplet population and elongation in both mono- and co-cultures.

Additionally, it is interesting to see the ability of the PDO monoculture to grow at a similar rate to the co-cultures. **(Figure 3)** Included as a negative control, PDO monoculture was provided with full PDO culture medium for the first 7 days, after which culture medium was changed to starvation medium to assess the growth dynamics in absence of growth factors provided by the medium or resident fibroblasts. Interestingly, the PDOs growth did not seem to be affected by the change of medium. PDxO06 and PDO03 monocultures were even able to restore tumour growth after oxaliplatin treatment, underlining the resistance to therapy of certain PDOs without the presence of CAFs. **(Figure 3C.1,2)**

Taken together, further research on the viability of CAFs in the 3D model could improve the co-culture model and will allow for accurate analysis of possible cluster-dependant growth dynamics in PDOs.

The comparability of the CAFs in our biobank to the CAFs present in patient tumours is a technical limitation of our biobank and requires further investigation. The CAFs in our biobank were obtained by culturing dissected fragments of tumour, and hereby selecting for CAF populations that were able to transfer from growing *in vivo* in tumour tissue, to *in vitro* in culture flasks. As each patient's CRC tumour will contain a heterogeneous population of CAFs, we might be selecting for a subset from the total pool of CAF types.[20 25] Similarly, the CAFs in our biobank will not necessarily be the most abundant CAF type in the patient's tumour. By comparing our CAF expression profiles to single cell RNA sequencing studies on whole CRC tumours, we can further confirm the representability of our clusters for the CAF population in tumours.[36 37] In addition, cluster markers will be identified to assess patient tumour tissue sections for presence and abundance of our clusters via immunostainings.

In conclusion, these results show promising signs of the impact of CAFs in the TME on the tumour. Refinement of our patient-derived TME model will provide further insights on the influence of the distinct CAF clusters found in our biobank. Distinguishing CAF subtypes that play important roles in the TME to protect the tumour against treatment or drive relapse are an important next step to discovering new biomarkers and improving localised CRC care.

Acknowledgements

Hereby, I would like to extend my gratitude to everyone involved in my internship at the Calon lab. Firstly, I thank Alex for welcoming me to his wonderful research group and for advising me on my project and career. I thank Jordi for not only supervising me on a daily basis and helping finalise the report, but furthermore for allowing me to discover all aspects of a researcher's life, guiding me in my project, and spending the extra time to ensure I feel satisfied and comfortable during my stay. Next, I would like to thank Anna and Alba for being with me in all ups and downs over the past months, making me laugh every day and teaching me some Catalan. I thank Jenni for always checking in on me during the long evenings of work and thank the lab collectively for the fruitful discussions and teachings, and moreover for welcoming me to Barcelona. Lastly, I thank Onno Kranenburg for accepting to review my report and attend my final presentation.

Methodology

Cell culture

CRC Patient-derived fibroblasts from our biobank were cultured as monolayers in 75 cm^2 flasks (Corning, Corning, NY, USA) at atmospheric O_2, 37°C, 5% CO_2 and a relative humidity of 95%. Fibroblasts were passaged by using 1,5ml trypsin (Life Technologies GmbH, Darmstadt, Germany) after a wash with PBS (Cultek S L, Madrid, Spain). Fibroblasts were incubated with trypsin for 5-10 minutes until fully detached from the flask, after which the reaction was quenched with fibroblast medium (described below) without FGF-2. Cell suspension was then centrifuged at 700rpm for 7:00 minutes to isolate the pellet which was subsequently replated. Fibroblasts were passaged upon reaching between 70% and 95% confluency, at a ratio of 1:2 to 1:3. Patient-derived fibroblasts were cultured in fibroblast medium; DMEM (Life Technologies GmbH); 10% FBS; 1% Glutamine and 20µg/mL FGF-2 (Peprotech, Rocky Hill, NJ, USA). Medium was refreshed twice per week.

Patient-derived organoids (PDOs) of CRC patients were grown embedded in 40µl of BME (Reduced Growth Factor Basement Membrane Matrix, Type 2; Bio-Techne R&D Systems S.L., Minneapolis, MN, USA) in 24-well plates at atmospheric O_2, 37°C, 5% CO_2 and a relative humidity of 95%. PDOs were cultured in PDO medium (Advanced DMEM/F12; Life Technologies GmbH) containing; 1x Normocin (InvivoGen, Toulouse, France); 1x Penicillin-Streptomycin (InvivoGen); 1x B-27 without retinoic acid (Life Technologies GmbH); 1x Glutamax (Thermo Fisher Scientific, Hampton, NH, USA); 1x N-2 (Thermo Fisher Scientific); 1,25 mM N-Acetyl-L-cysteine (Merck life science S.L.U, NJ, USA); 10uM ROCK inhibitor (Tocris Bioscience, Bristol, UK); 1µg/ml R-spondin (Peprotech); 500nM A83 (Tocris); 10uM P38 inhibitor (Merck life science); 100ng/ml Noggin (tebubio, Barcelona, Spain); 50ng/ml FGF-2 (tebubio) and 50 ng/ml EGF (Preprotech). Medium was refreshed twice per week.

For tumour cell growth experiments, three stably growing PDOs (PDO03, PDO13, PDxO06 were infected with a lentiviral vector encoding a fusion protein reporter construct of mCherry, firefly luciferase and an IRES-Zeocin resistance cassette, which where cloned under control of the Ubiquitin promotor in a FUW vector. [34] [35] Stable expression of the construct in PDOs was selected for by using Zeocin (InvivoGen).

PDO-Fibroblast Co-culture

3D co-cultures were established by seeding 6000 PDOs with 100000 Fibroblast (a 3:50 ratio) in 40µl BME (Bio-Techne R&D Systems S.L.) in clear 24-well plates and cultured with 500µl of PDO starvation medium as described below (refreshed twice per week). Co-cultures were provided with PDO starvation medium (DMEM/F12; 1x B-27 without retinoic acid; 1x Glutamax; 1x N-2; 1,25mM N-Acetyl-L-cysteine; 1x Normocin; 10uM ROCK inhibitor and 0.5ng/ml EGF). 2 µg/ml oxaliplatin was included when indicated. Oxaliplatin treatment was washed out with a single 1x DMEM/F12 wash when changed for PDO starvation medium without oxaliplatin.

Fibroblast monoculture experiments

Fibroblasts were seeded in 60mm diameter petri dishes and cultured with 2ml of fibroblast medium. On day 1, medium was changed to fibroblast starvation medium (DMEM; 0. 2% FBS; 1% glutamine and 1% penicillin-streptomycin) for 8 hours, after which CAFs were treated with 5µg/ml of oxaliplatin in fibroblast starvation medium. On day 4, medium with oxaliplatin was refreshed.

Microscopy

Images were taken with a ZEISS Axio Vert.A1 FL - Inverted LED Fluorescence Microscope, connected to a Axiocam 305 colour (Carl Zeiss AG, Jena, Germany). The ZEN 3.7 software (Carl Zeiss AG) was used for image capture. Exposure, white balance, and Blacks & Whites fit were all set to auto, with binning set to 1x1.

Luciferase experiments

3D PDO-fibroblast co-cultures, containing 300 tumour cells and 5000 fibroblasts, were seeded in 5µl of BME (Bio-Techne R&D Systems S.L.) in clear flat bottom 96-well white plates and cultured with 100µl of PDO starvation medium (refreshed twice per week). For control, PDO monocultures were cultured with basal PDO-specific medium for the first 7 days, after which it was provided with PDO starvation medium.
For luminescence readings, 50µl DMEM/F12 containing (15µl/ml) of Luciferin (Resem BV, Lijnden, Netherlands), was added and plates were measured using the Microplate Luminometer Orion II (Berthold Detection Systems, Pforzheim, Germany) and the Simplicity 4.2 software (Berthold Detection Systems).
For the TGFβ sensitivity assay, PDO monocultures of 300 tumour cells were cultured as described above with PDO medium without A83 (control condition), supplemented with either A83 or TGFβ. After 10 days, luciferase measurements were done as described above.

RNA extraction

For RNA extraction, samples were washed using PBS (Cultek S L) and recollected in 500µlTri reagent (Merck life science S.L.U). 3D cultures were resuspended to break the drop and homogenise the sample. CAF monocultures were recover from the culture dish with a plastic scraper and homogenised. Subsequent RNA isolation was performed using the RNeasy Micro Kit (QIAGEN, Hilfen, Germany) following manufacturer's specifications.

cDNA conversion

Reverse transcription to cDNA was performed using High-Capacity cDNA Reverse Transcription Kit (Applied Biosystems, Thermo Fisher Scientific, Pleasanton, CA, USA) following the manufacturer's instructions, to reach an cDNA concentration of 50ng/µl.

Quantitative real-time PCR

Quantitative RT-PCR was performed in a 7900HT Fast Real-Time System (Applied Biosystems, Waltham, MA, USA) using LightCycler 480 SYBR GREEN I master assays (Roche, Basel, Switzerland) following the manufacturer's instructions. 6µl probe mix (80% SYBR GREEN master mix, 10% forward primer, 10% reverse primer, both at 200nM) and 4µl sample cDNA (10ng/µl) for every reaction.

SYBR Green primers sequences were as follows:

PP1A (F: CCCACCGTGTTCTTCGACATT, R: GGACCCGTATGCTTTAGGATGA)
EPCAM (F: ATAACCTGCTCTGAGCGAGTG, R: TGCAGTCCGCAAACTTTTACTA),
TAGLN (F: ACCGTGGAGATCCCAACTG, R: CCATCTGAAGGCCAATGACAT),
ACTA2 (F: GTGTTGCCCCTGAAGAGCAT, R: GCTGGGACATTGAAAGTCTCA),
WNT5A (F: ATTCTTGGTGGTCGCTAGGTA, R: CGCCTTCTCCGATGTACTGC),
MMP1 (F: CACGCCAGATTTGCCAAGAG, R: GAGTTGTCCCGATGATCTCCC),
POSTN (F: CTCATAGTCGTATCAGGGGTCG, R: CCAGGGCAACATTCATATAACA),
FAP (F: GCTGGAGCTAAGAATCCCGTT, R: TGAACGAGTATGTTTGCAGTGG).

Quantitative RT-PCR Data were analysed in the SDS v2.4 software (Applied Biosystems) and normalised using PP1a as housekeeping gene reference.

Data visualisation

Data was visualised using Graphpad Prism 8.0.1 (Graphpad Software, San Diego, CA, USA) and Adobe Illustrator 21.0.0 (Adobe Systems, San José, CA, USA). For the heatmap displayed in **figure 2**, Rstudio 2022.07.1+554 (posit, Boston, MA, USA) was used. In the source code the following packages were used: tidyverse, ggplot2, preprocessCore, esquisse, and pheatmap.

Statistical analysis

Generally, all experiments and measurements were performed with 3 or more biological replicates. Statistical analyses of between-group differences were performed using an unpaired student's t test with Welch's correction in Graphpad Prism 8.0.1 (Graphpad Software).

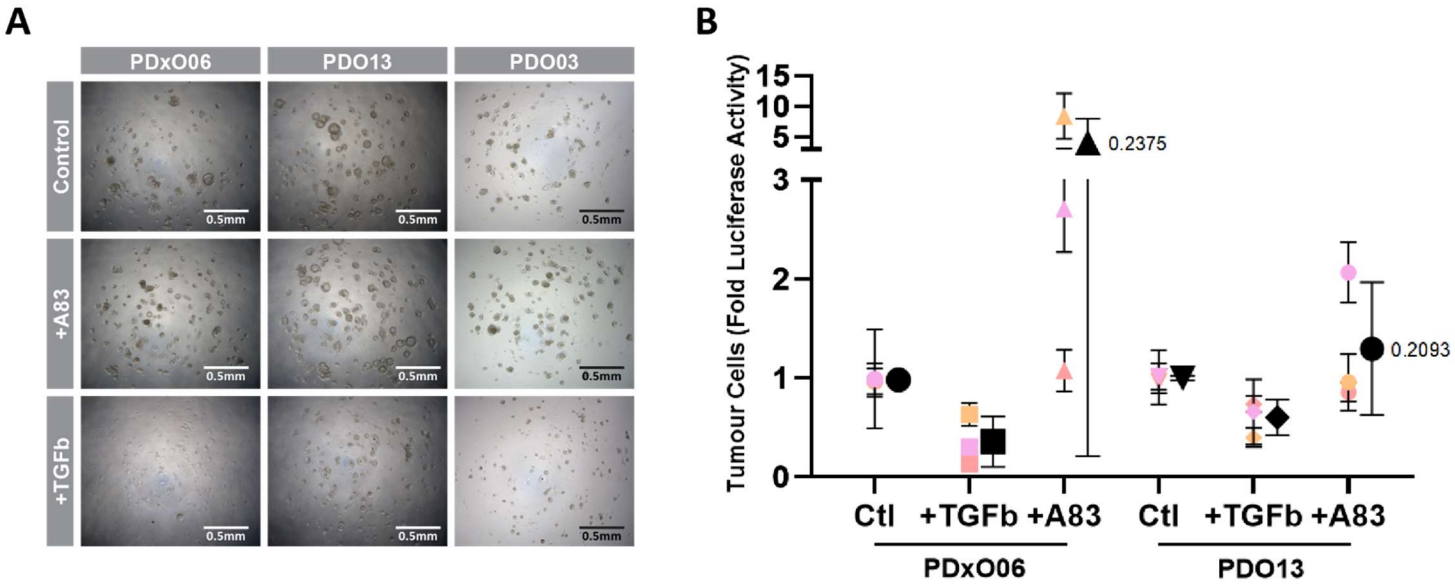

Supplemental figure 1

A) Bright field microscopy images of PDxO06, PDO13 and PDO03 3D monocultures after control, A83 and TGFβ treatments. **C)** Tumour growth of PDxO06, PDO13 and PDO03, as reported by fold increase in relative light units, indicating luciferase activity. PDO cultures were exposed to either a control medium, or medium containing A83 or TGFβ and measured on day 7. Colours represent different replicates ± SD, with black points representing the mean ± SD of all three replicates. P-values indicated derive from an unpaired t-test with Welch's correction to control conditions.

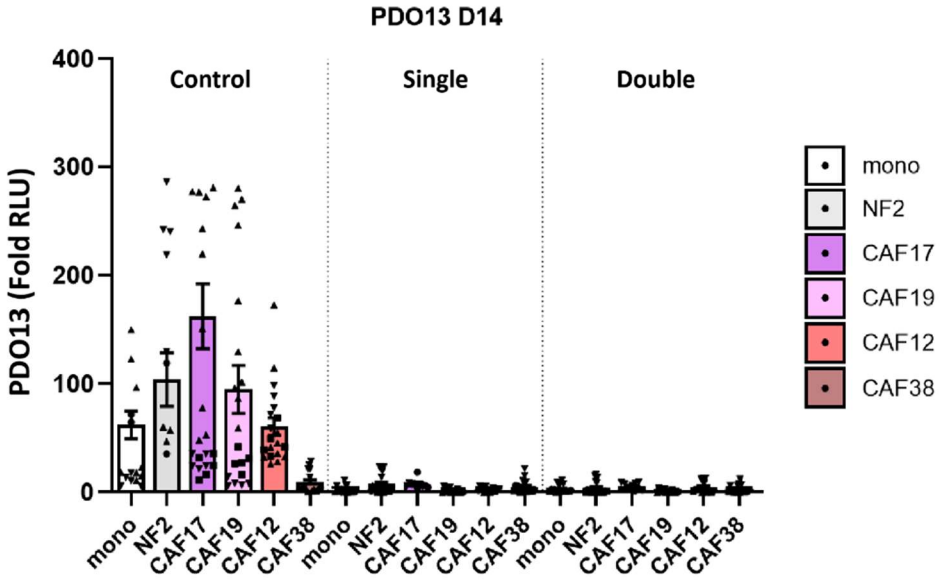

Supplemental figure 2

Tumour growth after 14 days for PDO13 under control, single or double chemotherapy treatment, as reported by fold increase in relative light units, indicating luciferase activity. Colours correspond to different co-cultures, as indicated in the legend. Each point presents an individual co-culture, with point shape corresponding to each replicate. Columns show mean values ± SEM.

Supplemental figure 3 (right)

10X bright field microscopy images of co-cultures with PDO3 and CAF03 or CAF05, in control, single and double oxaliplatin treatment conditions.

Supplemental figure 4 (below)

Fold relative gene expressions from patient-like co-cultures of PDO03 + CAF03 and PDO05 + CAF05 after 14 days of culturing, with control, single and double oxaliplatin treatment conditions. Points represent all qPCR replicates of 1 to 3 replicate experiments. Columns show mean ± SD, with colours corresponding to treatments. Genes plotted here are EPCAM as tumour cell marker (**A**), TAGLN and ACTA2 as cluster 1 markers (**B** cluster 1 indicated by purple border), WNT5A and MMP1 as cluster 3 makers (**C**, red), and POSTN and FAP as poor prognosis biomarkers (**D**).

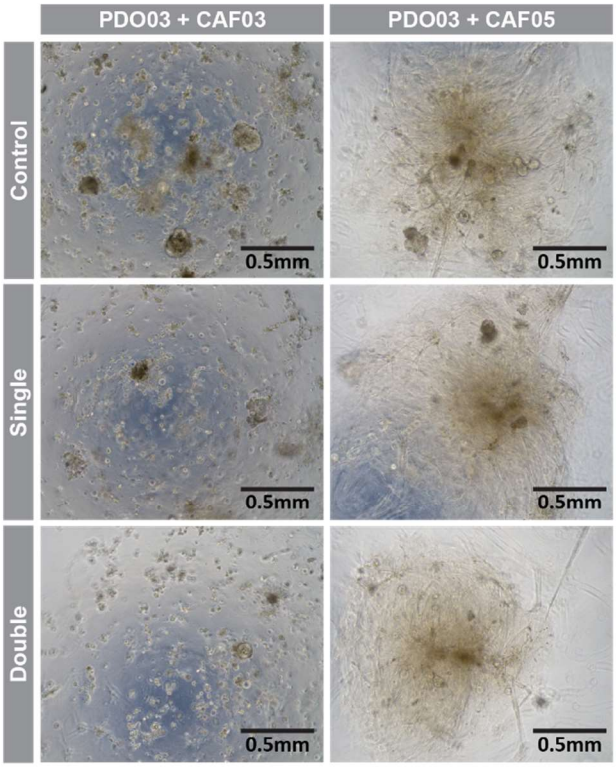

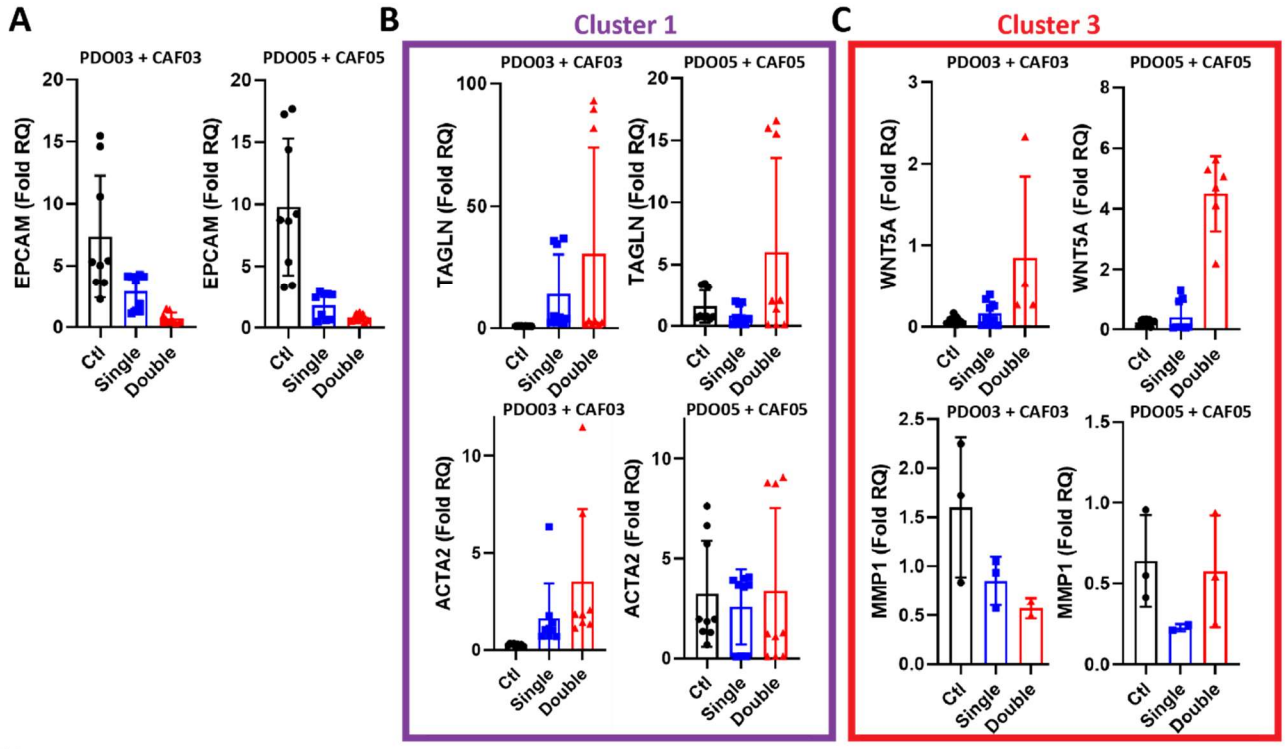

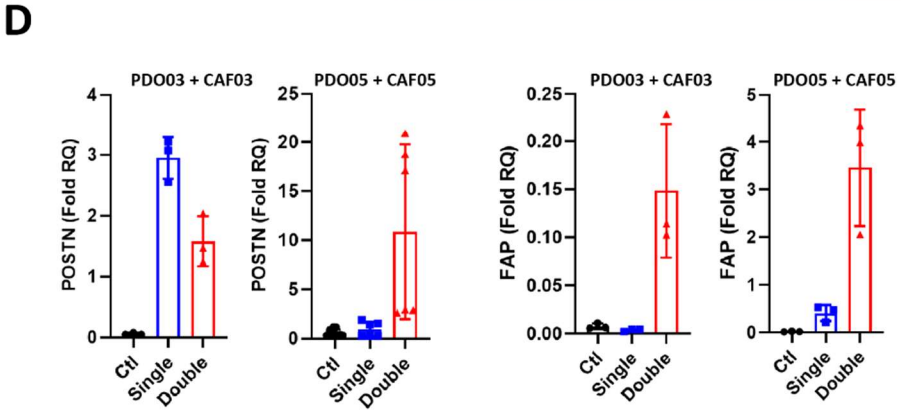

References

[1] Sung, H., Ferlay, J., Siegel, R. L., Laversanne, M., Soerjomataram, I., Jemal, A., & Bray, F. (2021). Global cancer statistics 2020: GLOBOCAN estimates of incidence and mortality worldwide for 36 cancers in 185 countries. *CA: a cancer journal for clinicians*, *71*(3), 209-249.

[2] Xi, Y., & Xu, P. (2021). Global colorectal cancer burden in 2020 and projections to 2040. *Translational oncology*, *14*(10), 101174.

[3] Kinzler, K. W., & Vogelstein, B. (1997). Gatekeepers and caretakers. *Nature*, *386*(6627), 761-763.

[4] Fearon, E. R., & Vogelstein, B. (1990). A genetic model for colorectal tumorigenesis. *cell*, *61*(5), 759-767.

[5] American Joint Committee on Cancer. Chapter 20 - Colon and Rectum. In: *AJCC Cancer Staging Manual*. 8th ed. New York, NY: Springer; 2017.

[6] Allemani, C., Matsuda, T., Di Carlo, V., Harewood, R., Matz, M., Nikšić, M., ... & Hood, M. (2018). Global surveillance of trends in cancer survival 2000–14 (CONCORD-3): analysis of individual records for 37 513 025 patients diagnosed with one of 18 cancers from 322 population-based registries in 71 countries. *The Lancet*, *391*(10125), 1023-1075.

[7] Kuipers, E. J., Grady, W. M., Lieberman, D., Seufferlein, T., Sung, J. J., Boelens, P. G., ... & Watanabe, T. (2015). Colorectal cancer. *Nature reviews. Disease primers*, *1*, 15065-15065.

[8] Dekker, E., Tanis, P. J., Vleugels, J. L., Kasi, P. M., & Wallace, M. Colorectal Cancer (2019). Pure-AMC. *Lancet*, *394*, 1467-80.

[9] Biller, L. H., & Schrag, D. (2021). Diagnosis and treatment of metastatic colorectal cancer: a review. *Jama*, *325*(7), 669-685.

[10] Guinney, J., Dienstmann, R., Wang, X., De Reynies, A., Schlicker, A., Soneson, C., ... & Tejpar, S. (2015). The consensus molecular subtypes of colorectal cancer. *Nature medicine*, *21*(11), 1350-1356.

[11] Dienstmann, R., Vermeulen, L., Guinney, J. *et al.* Consensus molecular subtypes and the evolution of precision medicine in colorectal cancer. *Nat Rev Cancer* 17, 79–92 (2017). https://doi-org.proxy.library.uu.nl/10.1038/nrc.2016.126

[12] Nagtegaal, I. D., Marijnen, C. A., Kranenbarg, E. K., van de Velde, C. J., van Krieken, J. H. J., & Pathology Review Committee the Cooperative Clinical Investigators. (2002). Circumferential margin involvement is still an important predictor of local recurrence in rectal carcinoma: not one millimeter but two millimeters is the limit. *The American journal of surgical pathology*, *26*(3), 350-357.

[13] van de Velde, C. J., Boelens, P. G., Borras, J. M., Coebergh, J. W., Cervantes, A., Blomqvist, L., ... & Valentini, V. (2014). EURECCA colorectal: multidisciplinary management: European consensus conference colon & rectum. *European journal of cancer*, *50*(1), 1-e1.

[14] Gelibter, A. J., Caponnetto, S., Urbano, F., Emiliani, A., Scagnoli, S., Sirgiovanni, G., ... & Cortesi, E. (2019). Adjuvant chemotherapy in resected colon cancer: when, how and how long?. *Surgical Oncology*, *30*, 100-107.

[15] Marques, R. P., Duarte, G. S., Sterrantino, C., Pais, H. L., Quintela, A., Martins, A. P., & Costa, J. (2017). Triplet (FOLFOXIRI) versus doublet (FOLFOX or FOLFIRI) backbone chemotherapy as first-line treatment of metastatic colorectal cancer: A systematic review and meta-analysis. *Critical reviews in oncology/hematology*, *118*, 54-62.

[16] Xie, Y. H., Chen, Y. X., & Fang, J. Y. (2020). Comprehensive review of targeted therapy for colorectal cancer. *Signal transduction and targeted therapy*, *5*(1), 22.

[17] Venook AP, Niedzwiecki D, Innocenti F, at al. Impact of primary (1°) tumor location on overall survival (OS) and progression-free survival (PFS) in patients (pts) with metastatic colorectal cancer (mCRC): analysis of CALGB/SWOG 80405 (Alliance). J Clin Oncol 2016; 34 (suppl 15): 3504 (abstr).

[18] Giantonio, B. J. et al. Bevacizumab in combination with oxaliplatin, fluorouracil, and leucovorin (FOLFOX4) for previously treated metastatic colorectal cancer: results from the Eastern Cooperative Oncology Group Study E3200. J. Clin. Oncol. 25, 1539–1544 (2007).

[19] Kubicka, S. et al. Bevacizumab plus chemotherapy continued beyond first progression in patients with metastatic colorectal cancer previously treated with bevacizumab plus chemotherapy: ML18147 study KRAS subgroup findings. Ann. Oncol. 24, 2342–2349 (2013).

[20] Colangelo, T., Polcaro, G., Muccillo, L., D'Agostino, G., Rosato, V., Ziccardi, P., ... & Colantuoni, V. (2017). Friend or foe?: The tumour microenvironment dilemma in colorectal cancer. *Biochimica et Biophysica Acta (BBA)-Reviews on Cancer*, *1867*(1), 1-18.

[21] Becht, E., de Reyniès, A., Giraldo, N. A., Pilati, C., Buttard, B., Lacroix, L., ... & Fridman, W. H. (2016). Immune and Stromal Classification of Colorectal Cancer Is Associated with Molecular Subtypes and Relevant for Precision ImmunotherapyDistinct Immune Phenotypes of Colorectal Cancer Molecular Subtypes. *Clinical cancer research*, *22*(16), 4057-4066.

[22] Karagiannis, G. S., Poutahidis, T., Erdman, S. E., Kirsch, R., Riddell, R. H., & Diamandis, E. P. (2012). Cancer-associated fibroblasts drive the progression of metastasis through both paracrine and mechanical pressure on cancer tissueinterdigital model of metastasis. *Molecular cancer research*, *10*(11), 1403-1418.

[23] Cirri, P., & Chiarugi, P. (2011). Cancer associated fibroblasts: the dark side of the coin. *American journal of cancer research*, *1*(4), 482.

[24] Hawinkels, L. J. A. C., Paauwe, M., Verspaget, H. W., Wiercinska, E., Van Der Zon, J. M., Van Der Ploeg, K., ... & Sier, C. F. M. (2014). Interaction with colon cancer cells hyperactivates TGF-β signaling in cancer-associated fibroblasts. *Oncogene*, *33*(1), 97-107.

[25] Kalluri, R. (2016). The biology and function of fibroblasts in cancer. *Nature Reviews Cancer*, *16*(9), 582-598.

[26] Linares, J., Marín-Jiménez, J. A., Badia-Ramentol, J., & Calon, A. (2021). Determinants and functions of CAFs secretome during cancer progression and therapy. *Frontiers in Cell and Developmental Biology*, *8*, 621070.

[27] Paunescu, V., Bojin, F. M., Tatu, C. A., Gavriliuc, O. I., Rosca, A., Gruia, A. T., ... & Vermesan, S. (2011). Tumour-associated fibroblasts and mesenchymal stem cells: more similarities than differences. *Journal of cellular and molecular medicine*, *15*(3), 635-646.

[28] Chen, Y., McAndrews, K. M., & Kalluri, R. (2021). Clinical and therapeutic relevance of cancer-associated fibroblasts. *Nature reviews Clinical oncology*, *18*(12), 792-804.

[29] Gascard, P., & Tlsty, T. D. (2016). Carcinoma-associated fibroblasts: orchestrating the composition of malignancy. *Genes & development*, *30*(9), 1002-1019.

[30] Oskarsson, T., Batlle, E., & Massagué, J. (2014). Metastatic stem cells: sources, niches, and vital pathways. *Cell stem cell*, *14*(3), 306-321.

[31] Calon, A., Lonardo, E., Berenguer-Llergo, A., Espinet, E., Hernando-Momblona, X., Iglesias, M., ... & Batlle, E. (2015). Stromal gene expression defines poor-prognosis subtypes in colorectal cancer. *Nature genetics*, *47*(4), 320-329.

[32] Linares, J., Sallent-Aragay, A., Badia-Ramentol, J., Recort-Bascuas, A., Méndez, A., Manero-Rupérez, N., ... & Calon, A. (2023). Long-term platinum-based drug accumulation in cancer-associated fibroblasts promotes colorectal cancer progression and resistance to therapy. *Nature Communications*, *14*(1), 746.

[33] Rivas, E. I., Linares, J., Zwick, M., Gómez-Llonin, A., Guiu, M., Labernadie, A., ... & Calon, A. (2022). Targeted immunotherapy against distinct cancer-associated fibroblasts overcomes treatment resistance in refractory HER2+ breast tumors. *Nature Communications*, *13*(1), 5310.

[34] Calon, A., Espinet, E., Palomo-Ponce, S., Tauriello, D. V., Iglesias, M., Céspedes, M. V., ... & Batlle, E. (2012). Dependency of colorectal cancer on a TGF-β-driven program in stromal cells for metastasis initiation. *Cancer cell*, *22*(5), 571-584.

[35] Lois, C., Hong, E. J., Pease, S., Brown, E. J., & Baltimore, D. (2002). Germline transmission and tissue-specific expression of transgenes delivered by lentiviral vectors. *science*, *295*(5556), 868-872.

[36] Qian, J., Olbrecht, S., Boeckx, B., Vos, H., Laoui, D., Etlioglu, E., ... & Lambrechts, D. (2020). A pan-cancer blueprint of the heterogeneous tumor microenvironment revealed by single-cell profiling. *Cell research*, *30*(9), 745-762.

[37] Lee, H. O., Hong, Y., Etlioglu, H. E., Cho, Y. B., Pomella, V., Van den Bosch, B., ... & Park, W. Y. (2020). Lineage-dependent gene expression programs influence the immune landscape of colorectal cancer. *Nature genetics*, *52*(6), 594-603.